Controls on the grain size distribution of landslides in Taiwan: the influence of drop height, scar depth and bedrock strength.

Odin Marc[1, 2], Jens M. Turowski[2], and Patrick Meunier[3]

[1]Géosciences Environnement Toulouse (GET), UMR 5563, CNRS/IRD/CNES/UPS, Observatoire Midi-Pyrenees, 14 Avenue Edouard Belin, 31400 Toulouse, France.
[2]German Research Center for Geoscience, GFZ-Potsdam, Section 4.6, Geomorphology, Telegrafenberg, Potsdam, Germany
[3]Laboratoire de Géologie, Ecole Normale Supérieure, 15 Rue Lhomond, Paris, France

Correspondence: Odin Marc, odin.marc@get.omp.eu

Abstract. The size of grains delivered to river by hillslopes processes is thought to be a key factor to better understand sediment transport, long-term erosion as well as sedimentary archives. Recently, models have been developed for the grain size distribution produced in soil, but they may not apply to active orogens where high erosion rates on hillslopes are driven by landsliding. Until now relatively few studies have focused on landslide grain size distributions. Here we present grain size

5 distribution (GSD) obtained by the grid-by-number sampling on 17 recent landslide deposits in Taiwan, and we compare it to the geometrical and physical properties of the landslides, such as their width, area, rock-type, drop height and estimated depth. All slides occurred in slightly metamorphosed sedimentary units, except two, which occurred in younger unmetamorphosed shales, with rock strength expected to be 3 to 10 times weaker from their metamorphosed counterparts. We found that 4 deposits displayed a strong grain-size segregation on their deposit with downslope toe deposits 3 to 10 times coarser than apex

10 deposits. In 3 cases, we could also measure the GSD inside the landslides that presented percentiles 3 to 10 times finer than the surface of the deposit. Both observations could be due to either kinetic sieving or deposit reworking after the landslide failure but we cannot explain why only some deposits had a strong segregation. Averaging this spatial variability we found the median grainsize of the deposits to be strongly negatively correlated to drop height, scar width and depth. However, previous work suggest that regolith particles and bedrock blocks should coarsen with increasing depth, opposite to our observation.

15 Accounting for a model of regolith coarsening with depth, we found that the ratio of the original bedrock block size and the D50 was proportional the potential energy of the landslide normalized to its bedrock strength. Thus the studied landslides agree well with a published, simple fragmentation model, even if that model was calibrated on much larger and much stronger rock avalanches than those featured in our dataset. This scaling may thus serve for future model of grain size transfer from hillslopes to river, trying to better understand landslide sediment evacuation and coupling to river erosional dynamics.

1 Introduction

Grain size is an essential parameters to understand sediment transport and associated issues in river evolution or hazard related to sediment pulses. For geomorphologists, it is increasingly considered an important parameter for the long-term incision of bedrock streams (Sklar and Dietrich, 2001; Cook et al., 2013, 2014; Turowski, 2018), while it is an essential part of the sedimentological signal which is ultimately archived in sedimentary structure (e.g., Armitage et al., 2011).

5 Still, there are many processes that control the grain size distribution (GSD) in rivers, and they are poorly understood (Allen et al., 2015). In recent studies models have been proposed describing how weathering in the critical zone reduced the original size distribution of bedrock before the grains reach the surface (Marshall and Sklar, 2012; Riebe et al., 2015; Sklar et al., 2017). However, in active orogens with high erosion rates (>0.5 mm/yr), landslides are likely the main providers of sediments to rivers

10 (Hovius et al., 1997; Struck et al., 2015; Marc et al., 2019), and a large fraction of sediment may reach the river incompletely weathered. Indeed, the limits of models predicting soil GSD and the need to account for GSD derived from fractured bedrock was recently shown (Neely and DiBiase, 2020), though the role of mass wasting in delivering and further fragmenting bedrock particles was not explored. In those settings, understanding and modeling the controls on landslide GSD should be an urgent goal, which has been addressed by few studies. Indeed, in contrast to river sediments for which many studies exist (e.g.,

15 Ibbeken, 1983; Whittaker et al., 2011; Chung and Chang, 2013; Guerit et al., 2014, 2018) landslide GSDs have rarely been measured, in part because the latter is considerably more difficult, time consuming and potentially dangerous than the former. A few studies have measured and discussed in detail the GSD of some large historical landslide or rock avalanches, often putting forward the various mechanism of rock fragmentation and grain segregation (see Crosta et al., 2007, and references therein). Although interesting for their discussion in terms of rock mechanics, such case studies did not allow to understand the regional

20 variability of landslide GSDs, nor to derive physical scaling that could pave the way to model the GSD of material delivered to river networks by landslides. To our knowledge only seven studies reported detailed GSD measurements from multiple landslide deposits. A pioneering study reported the GSD from 42 landslide dams across the Appenines, with a discussion on the methods to derive the GSD but none on the controls of the GSD variability (Casagli et al., 2003). Locat et al. (2006) presented GSDs from nine large ($> 100 \ Mm^3$) rock avalanches from Canada and the Alps, including various rock types,

25 were presented and analyzed in terms of potential energy and fragmentation theories (Locat et al., 2006). They found that the ratio of bedrock initial median block size, D_i (estimated from fracture spacing), and the deposit median grain size, D_{50}, was proportional to the change in potential energy per unit of volume, $\rho g H$, normalized by the point-load strength of the bedrock, σ_c. Specifically their nine rock avalanches were best fit by a relation that could be recast as:

$$D_{50} = \frac{D_i}{k_1 \frac{\rho g H}{\sigma_c} - k_2} \tag{1}$$

With $k_2 = 0.5$ an empirical threshold for fragmentation, and $k_1 = 83.3$ an empirical coefficient relating to the conversion of

30 potential energy into fragmentation energy and the effective breaking of particles. Thus, if the scaling is general for landslide, the deposit D_{50} should increased with the source block size and the rock strength but decrease with the drop height of the center of mass, H. However, subsequent studies often focused on the potential importance of landslide GSD to understand sediment

transport dynamics and the expected GSD at the outlet of basins and reported GSDs in Nepal, Japan, California and Southern Italy (Attal and Lavé, 2006; Nishiguchi et al., 2012; Attal et al., 2015; Roda-Boluda et al., 2018). Several of them underlined, qualitatively, the factors influencing the GSDs such as the different lithological units (Attal and Lavé, 2006; Roda-Boluda et al., 2018), or the local hillslope gradient (Attal et al., 2015). Very recently a study presented the GSD of seven medium size

5   rockfalls in Spain, showing that the bedrock block size and the deposit GSD could be related through a fractal fragmentation model (Ruiz-Carulla and Corominas, 2020). They found that potential energy was a main control on the fragmentation, but no clear correlation with rock strength measurements emerged. They did not compare their model and result to the simple scaling proposed by Locat et al. (2006). Thus, none of these more recent works has attempted to frame the landslide GSD in terms of the competition between fragmentation energy and source rock strength, and the scaling for large rock avalanches has not been

10 reproduced on smaller, more common landslides.

Based on these studies we formulate two hypotheses. First, we suggest that Eq (1) could be generalized to intermediate size and depth landslides, and thus that landslide D_50 should increase with rock strength, σ_c, and source materials median size D_i, but decrease with drop height, H. Second, that materials mobilized by shallow landslides coarsen with the landslide scar thickness, T, (i.e.,D_i increases with T), due to a reduction of the fracture density (Clarke and Burbank, 2011) and/or of the degree of

15 physical and chemical weathering experience by particles (Cohen et al., 2010; Anderson et al., 2013; Sklar et al., 2017). Testing these hypotheses seems essential to pave the way towards geomorphic models accounting for the GSD of sediments transferred from hillslopes to river and from river to sedimentary basins (Allen et al., 2015; Sklar et al., 2017).

With these goals, and given the sparse amount of data on landslide GSDs, we performed detailed measurements on 17 recent landslide deposits in Taiwan. Taiwan is a prime example of an active mountain belt where landslides are the main supplier

20 of sediment to rivers (Hovius et al., 2000) and where river GSDs exist in the literature (Chung and Chang, 2013; Lin et al., 2014). Still, to our knowledge, comprehensive landslide GSD measurements are still lacking in Taiwan. Below we report our measurements, discuss the source of variability of the GSD within given landslides and across the whole dataset. Then, we discuss the validity of the two hypothesis stated above based on the GSD of these landslides. We end by discussing the implications in terms of caveat and opportunity for GSD sampling and implications for fluvial sediment transport.

2   Data and Methods

In this study we report original GSDs for 17 landslide deposits from Taiwan (Fig 1), as well as basic landslide information that we use to discuss controls on the GSD (Table 1). We detailed below how we constrained landslide characteristics for each deposits and how we measured GSD for each deposits.

2.1   Landslide characteristics

30 To quantify the variability in landslide GSD and its controls, we have targeted landslides with a known triggering date, and covering a broad range of sizes and lengths. Except for four small landslides, which were opportunistically sampled in parallel of larger neighbouring ones, all landslides were targeted based on satellite imagery and chosen for the accessibility of their

deposit. Out of 17, 13 were chosen in the same geographic area and lithological unit, on both side of the southern section of Taiwan Central Range (Fig 1), allowing to have a variability in GSD independent of rock type. The four remaining landslides occurred in other lithological units. Specifically, LS-10 occurred in the emergent topography of Taiwan southern tip, LS-15 and LS-1 on both side of the northern part of the Central Range, and LS-16 in the Northwestern foothills. Landslide type

5 was difficult to assess, but all landslide could be called disrupted landslides, involving a mixture of regolith and bedrock. The only exception is LS-12, the largest event which may rather be a deep slump with moderate displacement and probably some rotational components. Most landslides correspond to landslide polygons present in the Typhoon Morakot landslide inventory (Marc et al., 2018), and thus occurred in August 2009, about five and a half year before they were surveyed in March 2015. Other more recent landslides were dated based on the time-series of images available in Google Earth (see Table 1). Based

10 on the geological map of Taiwan (available from Taiwan Central Geological Survey), we assign each landslides to a geological formation and the associated rock-type (Fig 1, Table 1). Most landslides (13) are in the Lushan formation, composed of slate and slightly metamorphosed sandstone. Two of the four remaining landslides are also in metasedimentary units, LS-1 in black schist and LS-15 in metasandstone intercalated with slate. Then, the two last landslides occurred in non metamorphosed units, LS-10 is in the Nanchuang formation, alternating sandstones and shales, and LS-16 in the Cholan/Chinshui shale. In

15 LS-16 the high abundance of clay made weak agglomerate that could be broken with hands, highlighting the weakness of this unit compared to the other landslides. In an effort to associate these formations to quantitative strength estimates, we refer to measurements reported for 128 samples from the Chenyoulan catchment, both for the Nanchuang formation and the metasediments where LS-15 occurred (Lin et al., 2008). The unconfined compressive strength of Nanchuang sandstone ranged from 29 to 117 MPa (mean of 70 MPa), while the metasandstone units ranged from 45 to 179 MPa (Mean of 100 MPa). However,

20 shales are about equally represented than sandstone in the Nanchuang formation, with strength below 10 MPa, while the slates intercalated with the metasandstone are more irregular and presumably stronger. These measurements clearly make the case for highly variable rock strength and are far from encompassing the potential diversity of rock-type sampled by the studied landslides. Still to first order, we expect LS-16 to be very weak, with strength about 10 MPa, LS-10 to have strength around 30 MPa (with large uncertainties depending if the strength is rather dominated by the shale or the sandstone), and the rest of

25 the landslide from metasedimentary units, to be stronger than around 100 MPa. The point load strength, σ_c, is typically 15 to 25-fold smaller than the unconfined compressive strength (Chau and Wong, 1996) and therefore we consider $\sigma_c \sim 5\,MPa$ for the landslides in metasedimentary units and $\sigma_c \sim 1.5\,MPa$ and $\sigma_c \sim 0.5\,MPa$, for LS-10 and LS16 respectively.

Geometric landslide metrics were obtained from high resolution satellite imagery available in Google Earth except for four

30 (LS-4, 9n, 13 and 14) deposits which were too small to be clearly distinguished on the imagery, and which had their dimensions approximated from field observations only, using a laser ranger. Area was obtained by hand mapping the whole disturbed zone on the imagery. Length refers to the downslope length between the highest and lowest point of the polygon. The elevation difference between these two points, estimated from the elevation data of Google Earth (in Taiwan mostly 30m SRTM), defined the maximum drop height. The scar width was obtained by measuring the extent of the landslide in the direction or-

35 thogonal to flow, in the upper part of the failure only. A smaller drop height and length were obtained when considering the

location of the estimated center of mass of the scar and deposits, estimated in Google Earth based on the imagery. An estimate of scar slope could be derived from the scar approximate length and height difference. For all landslides we estimated the upper, respectively lower, volume of the landslide using empirical scaling relationships with the scar area A_s, of the form $V = \alpha A_s^\gamma$, assuming the scar was mobilizing bedrock or soil, respectively (Larsen et al., 2010). We used $\gamma = 1.262 \pm 0.009$ and $log10(\alpha) = 0.649 \pm 0.021$ for the soil assumption, and $\gamma = 1.41 \pm 0.02$ and $log10(\alpha) = 0.63 \pm 0.06$ for the bedrock assumption. Then we derived the upper and lower estimate of landslide mean scar depth as the ratio of volume for bedrock and soil, respectively, and scar area. For this we estimated scar areas as $A_s = 1.5W_s^2$, consistent with global landslide geometry database (Domej et al., 2017), except for a few landslides where direct observations of the scar dimensions did not match this simple scaling (Table 1). Last, for a few landslides the deposit volume could be approximated as a fraction (a quarter to a half) of a cone, for which a volume estimate could be obtained as $\pi R^2 h/3$ with R and h the approximate radius and height of the cone which were estimated in the field. This simplified geometry was only suitable for LS-3, 4, 7, 9n, 10, 11, 13 and 15, and yield only a 1st order volume estimate (Table 1). Nevertheless, these field estimates mostly fall within the bracket of the volumes estimated from global scaling relationships, lending some support to this approach. Also note that LS-3 and LS-4, in which fresh vegetation debris was still present and a yellowish rock colour indicated advanced weathering (See Fig 1) had their field estimate similar to the soil scaling while for LS-7 and LS-11, which were clearly involving mostly fresh bedrock, the field volume matches better the bedrock scaling. Thus, to better capture the variability of landslide scar depth for the landslides without field volume estimate, we either applied the bedrock scaling or the averaged the soil and bedrock scaling, depending on the landslide characteristic. We used the bedrock estimate for the largest landslides ($W_s > 50$) within which the rock looked mostly fresh (i.e., LS-1, 2, 8, 12). For the other, smaller landslides (LS-5, 6, 9o,) and for LS-16, we averaged the bedrock and soil thickness estimates. These estimates (together with the ratio of field volume and scar area) are considered best estimate for the scar thickness (Table 1).

When we give a value with uncertainties on correlation index (Pearson's R or R^2) they always refer to the mean and standard deviation from 10,000 random bootstrapped subsamples of the considered sample.

2.2 Grain size counting

GSDs were obtained using the grid-by-number sampling, following established protocols developed for measuring riverine GSDs (see, Kellerhals and Bray, 1971) and subsequently applied to landslide deposits (Casagli et al., 2003; Attal and Lavé, 2006). We extended survey tapes along a substantial portion of the deposit width (10 to 50m) and sampled grains along the tape at a constant interval, recording the size bin of b-axis measured with rulers. We used bins following a half Phi scale (power of 2 by 0.5 increments) with the smallest bins encompassing all grains finer than 2 mm. When grains could not be moved we considered the smallest of the two visible axis as the b-axis. The grid step was 0.5 m in most cases but was adjusted to 1 meters for deposits where many meterscale boulder where present (LS-2s, LS-13, LS-14) to limit the number of time when a grain would be counted several times. Then we moved the line in parallel, upslope by one to a few meters depending on the deposit dimensions and local topography, and repeated the counting. Most slides where sampled with 6-10 survey lines allowing to cover

Table 1. Landslide characteristics for the 17 surveyed deposits. Asterisks indicate landslides for which the geometry was estimated in the field rather than from satellite imagery. Due to its complex displacement LS-12 has large uncertainties on the displacement of its center of mass. Bsc=Black schist (Tananao Fm); Sl/Sd= Slate/Sandstone (Lushan Fm); Sh/Sd=Shale Sandstone (NanChuang Fm) ; Msd=Metasandstone (ShihPachungshi Fm); Sh=Shale (Chinshui/Cholan Fm).

Ldsl No	1	2	3	4*	5	6	7	8	9o	9n*	10	11	12	13*	14*	15	16
Landslide Length, Lmax (m)	192	400	100	25	125	25	135	330	120	15	60	270	330	20	10	310	160
Horizontal displacement of the center of mass, L (m)	100	330	70	15	95	15	90	250	85	8	40	220	120 ±50	10	5	240	90
Scar Width, W, (m)	80	90	60	20	30	15	35	70	25	5	20	60	280	15	10	180	80
Area, A, (m^2)	13171	33583	7801	756	2228	538	6115	14523	1834	40	921	18196	104454	300	150	58751	15214
Longitude (°)	121.415	120.948	120.896	120.894	120.857	120.857	120.899	120.852	120.857	120.857	120.775	120.657	120.679	120.681	120.681	120.902	120.833
Latitude (°)	23.734	22.597	22.516	22.514	22.439	22.435	22.508	22.438	22.435	22.435	22.135	22.444	22.519	22.517	22.516	23.609	24.286
Center of Scar Elev. (m)	560	380	200	175	300	285	480	420	305	282	240	265	460	415	430	1050	450
Center of Deposit Elev. (m)	485	130	160	160	240	270	410	300	275	275	225	155	390	405	410	870	405
Drop of the center of mass, H, (m)	75	250	40	15	60	15	70	120	30	7	15	110	70 ±30	10	20	180	45
Maximum Drop, Hmax, (m)	130	320	60	20	70	25	120	170	40	12	25	180	180	20	25	260	70
Scar Gradient	1	0.9	0.6	0.6	0.9	1	1.2	0.8	0.8	0.8	0.6	1	0.55	2.15	2.15	1	0.6
Volume (W-B scaling), V, (m^3)	96606	134664	42922	1937	6078	861	9388	66293	3635	39	1937	42922	3305783	861	274	950949	96606
Volume (W-R scaling) , V, (m^3)	15405	20728	7461	468	1301	227	2904	11003	822	14	468	7461	362004	227	82	118894	15405
Thickness (W-B scaling), (m)	10.06	11.08	7.95	3.23	4.5	2.55	5.1	9.02	3.88	1.04	3.23	7.95	28.11	2.55	1.83	19.57	10.06
Thickness (W-R scaling) (m)	2.43	2.58	2.09	1.18	1.46	1.02	1.6	2.27	1.33	0.57	1.18	2.09	4.66	1.02	0.82	3.7	2.43
Occurrence Year	2013.5	2012.5	2014.7	NA	2009.5	2009.5	2009.5	2009.5	2009.5	NA	2013.5	2009.5	2009.5	NA	NA	2014.8	2013.5
Rock type	Bsc	Sl/Sd	Sl/Sd	Sl/Sd	Sl/Sd	Sl/Sd	Sl/Sd	Sl/Sd	Sl/Sd	Sl/Sd	Sh/Sd	Sl/Sd	Sl/Sd	Sl/Sd	Sl/Sd	Msd	Sh
Field Volume (m^3)			16000	850			12500			24	750	43000		600	115	550000	
Best Thickness (See Methods), T, m	10.06	11.08	2.96	1.42	2.98	1.78	6.8	9.02	2.6	0.64	1.25	7.96	28.11	1.78	0.77	11.32	6.25

substantial fraction of the deposit (often 30 to 60%), with total counts often $> 200 - 400$ individual grains. This approach also allowed to sample different section of the deposit when a spatial segregation was visible (LS-3, LS-8, LS-9n, LS-10), and to quantitatively assess this spatial variability in grain size (see, Ruiz-Carulla et al., 2015). For two landslides we could separately count grains from the surface and from the interior of the deposit, counting grains on the vertical banks of a 2m deep erosional

5 gully incising the deposit of LS-8 and counting grains on a debris fan next and below the road that had been cleared from the deposit of LS-2. Thus the former case allowed us to survey the internal GSD, in place, while the latter more likely represent a remixing from surface and internal part, but which must, by volume and number be more representative of the inner GSD. Note that for LS-2 the only undisturbed deposit was the one in the transport channel, where a carapace (a layer of very coarse grains, (Crosta et al., 2007)) seems to have formed (Fig. S1). Finally, on LS-5 we measured separately a debris fan and the

10 terminal section of a channelized deposit which was visibly coarser (Fig. S2). In this case, given the age of the deposit and its direct contact with the floodplain, it is plausible that the deposit was partly eroded and the fan may be a mixture of internal and superficial material, whereas the higher up channel section may be more representative of the original surface of the deposit. This will be further discussed when talking of segregation. Additionally, on the deposit of LS-7 we could distinguished by visual inspection grains made of slate, which were dark, elongated and without visible internal structure, from grains made of

15 metasandstone which were lighter, more cubic and with visible internal grains. We have counted them separately as we found them over the deposit. In many other deposits a large majority of grains either looked fairly homogeneous, or because of lack of time their systematic counting within different rock-type could not be done.

Earth **Surface**
Dynamics
Discussions
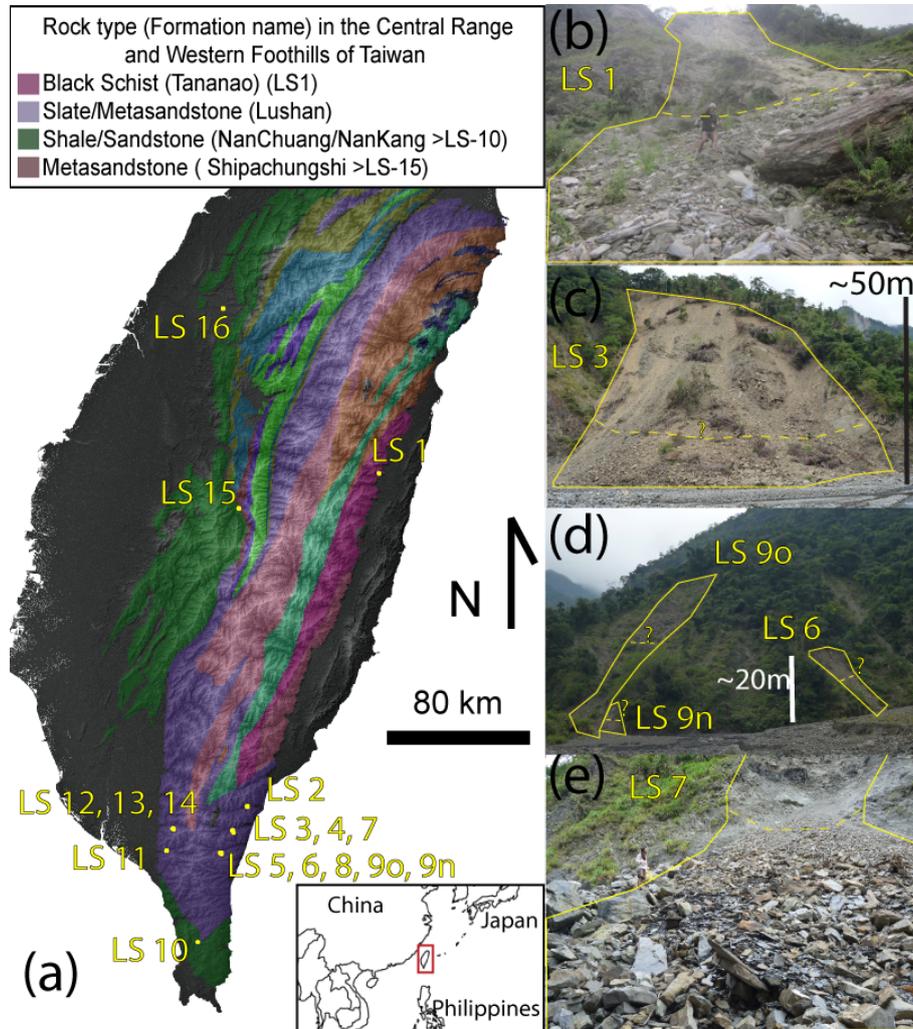
Figure 1. (a) Hillshaded elevation map of Taiwan, with the main lithological units of the central range and the locations of the 17 sampled landslides deposits. (b-e) pictures of some sampled landslides, where the yellow line is the approximate contour of the landslide (sometimes going beyond the pictures), and the dashed line indicate the transition from deposit to scar (it is only tentative when associated with "??"). In (b) and (e) the lead author is standing on the deposit for scale.

3 Results

3.1 Landslide grain size distributions and their internal variability

The landslide GSDs have a 50th and 84th percentiles ranging from $\sim 15 - 200 \ mm$ and $\sim 60 - 600 \ mm$, respectively. This is consistent with the range of observations from previous studies, except the large rock avalanches from Locat et al. (2006) and the volcanic rock avalanches Crosta et al. (2007), which were about 10 times coarser, respectively finer, than all other

Earth **Surface**
Dynamics
Discussions
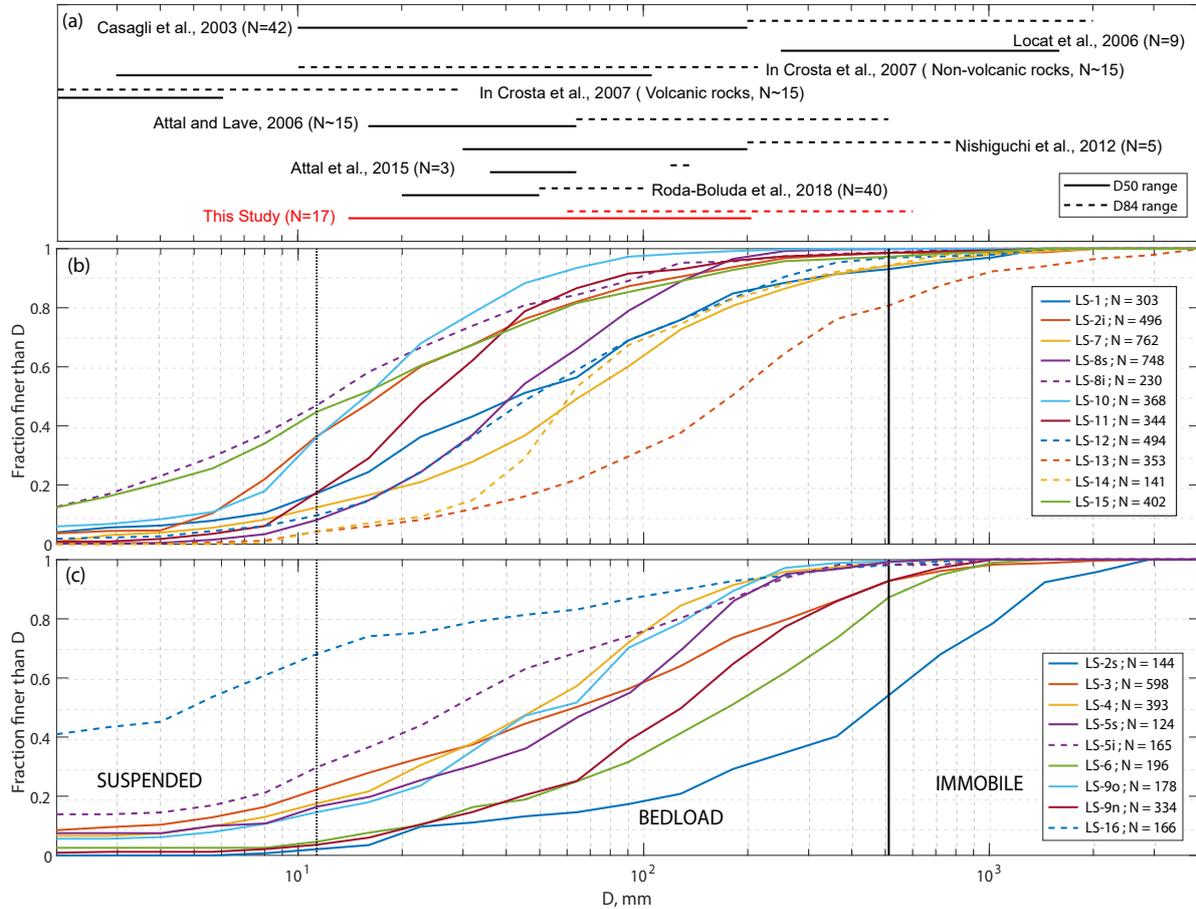
Figure 2. (a) range of D_{50} and D_{84} for various studies, excluding the coarsest and finest distributions of each study, and Cumulative distribution function for the 16 sampled landslide deposits. For visibility, panels (b) and (c) show distributions best fit by a log-normal distribution and a Weibull distribution, respectively. Note that LS-16 is poorly fit by both distributions. Vertical lines are approximate boundary for grain transport by suspension and bedload, for a flood associated with fluid shear stress of 220 Pa (see section Implications for sediment transport).

studies. LS-2s and LS-16 are much coarser and finer than the rest of the studied landslides, respectively. Interquartile ratios vary between 3 and 15, but we note that 13 out of 19 GSD have an interquartile ratio of 3 to 6, while only LS-1, 3, 5, 8i, 15 and LS-16 have larger spreads (Fig 2). All distributions seem unimodal, except LS-16 with more than 40% of the grains finer than 2 mm, likely containing a second, sub-millimetric mode that could not be constrained by our methods. Grain size distributions can often be well described by a Weibull or Lognormal distribution (Ibbeken, 1983). For the studied landslides, eight GSDs are better fit (according to both Kolmogorov-Smirnov and Anderson-Darling statistics, (Stephens, 1974)) by a Weibull distribution (LS 2s, 3, 4, 5s, 5i, 6, 9n, 9o), while all others are better fit by a log-normal distribution (Fig 2). Given these two subgroups we refrained from using parameters associated with one or the other distribution and will continue to discuss results based on

Earth **Surface**
Dynamics
Discussions
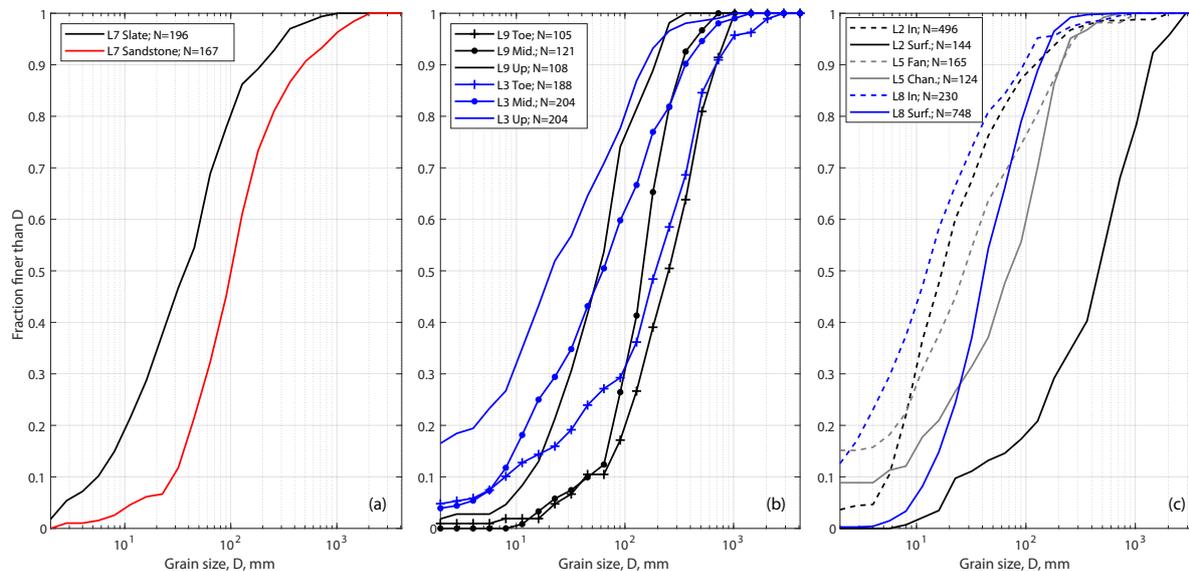
Figure 3. Three examples of heterogeneity in grain size distributions. (a) lithological difference within the deposit of LS-7 with sandstone grains coarser than slate grains. (b) Downslope differences between the upper, middle and lower part of the deposits of LS-3 and LS-9. (c) Difference between the surface and inner part of the deposits of LS-2, LS-5 and LS-8.

empirical descriptors (i.e., median, interquartile ratio).

GSDs within a single landslide deposit were often heterogeneous, in one case associated with differences between grains of different rock type (slate and sandstone in LS-7), while in seven other cases associated to spatial variability (Fig 3, S2).

5 For LS-7, the slate pieces have grain sizes about three times smaller than the sandstone for a given quantile of the CDF, with a similar distribution shape. The slate grains were typically elongated platelets (i.e., $a \sim 3b$ and $b >> c$), while the sandstone grains were cubic and slightly more abundant than the slate grains (N=196 vs N=167). We observed by naked-eye downslope segregation, i.e., an increase in sediment coarseness from the apex to the toe of the deposits (Ruiz-Carulla et al., 2015), for four cases. The strongest segregation occurred in deposits LS-3 and LS-9n, where the upper part of the deposits have grains

10 5-10 times finer than the lower part of the deposit, without changing substantially the shape of the distribution. Deposits LS-8 and LS-10 exhibited a more subtle segregation with the upper part of the deposits having distributions finer by a factor 1.5-2 in comparison to the toe of the deposits (Fig S2). The toe of LS-10 also displays D_{50} and D_{84} twice coarser than at its apex, consistent with other cases, but also has more fine grains, with about 10% of grains finer than 2 mm against less than 5% at the apex. The upper, middle (when differentiated) and lower sections of the deposits represented roughly similar proportion of the

15 surface of the deposits, and we obtained count variations below 10% from the different subsections (Fig 3). Therefore, to study the variability between various landslides we obtained an overall GSD by summing the grain counts from different sub areas

of the deposits with spatial segregation.

Then, in two cases we could separately measure the superficial and internal GSD. For LS-8 we observed that the superficial GSD had $D_{16} = 20\ mm$, $D_{50} = 40\ mm$ and $D_{84} = 120\ mm$ while the internal GSD had $D_{16} = 3\ mm$, $D_{50} = 10\ mm$ and

5 $D_{84} = 50\ mm$. There the superficial deposits had almost no fine sediment below 2mm, whereas the internal body had more than 10% of fine sediments. Thus, the internal GSD had quantiles 10 to 20 times finer than the channel carapace, the largest difference observed in terms of internal variability. Note that the carapace had also a coarser GSD than any other measured landslide deposit in our study. In spite of this massive difference we note that the internal GSD still had only about 3% grains finer than 2mm. These two examples clearly show that the superficial GSD can be substantially different from the internal

10 GSD, both in terms of fine grains (<2 mm) but also for coarse to very coarse grains (10 to 100 mm).

Last, in the case of LS-5, it is not entirely clear if the two distributions represent vertical segregation or superficial variability. Given its similar geometry (with a coarser channel than can be seen above, Fig. S4) with LS-2, and given the fan has a $D_{16} = 4\ mm$ and a $D_{50} = 20\ mm$, about three times finer than in the channel but an almost identical D_{84} around 200 mm, we consider it to likely be an internal or mixed GSD.

15 ## 3.2 Relations with landslide properties

The percentiles of the GSDs are highly correlated with linear correlation coefficients $R^2 > 0.9$ between D_{50} and D_{25}, D_{75}, D_{84} and D_{90}. However, two other metrics are poorly correlated to the D_{50}, the fraction of fine grains (here considering grains $< 8\ mm$) and the interquartile ratio (here D_{75}/D_{25}) characterizing the span of grain size in the distribution.

For the two landslides for which we have both an internal and superficial grain counting, we only considered one GSD. For

20 LS-8 we considered the superficial one, to be consistent with all other cases. In contrast for LS-2 we considered the internal GSD, because the superficial measurement recorded only what seems to be a carapace over-representing coarse grains. For LS-5 we considered the coarser distribution from the channel as more representative of the surface deposit. In case this would be due to spatial segregation and the fan distribution would actually represent the average surface the percentiles would be about twice finer, while the opposite is true for LS-2i which may have had a deposit 2-3 times coarser.

25

The drop height, H has the highest, negative, correlation with D_{50} ($R^2 = 0.71 \pm 0.13$; $N = 17$ with both terms log-transformed, Figure 4), with a best-fit power-law exponent -0.78. This correlation and exponent are obtained when rescaling the drop height of LS-10 and LS-16 by a factor 3.3 and 10, given their strength is 3.3 to 10 times smaller than for the metasedimentary units where the other landslides occurred. If instead we only fit the 15 deposit from the metamorphosed units we obtain $R^2 = 0.71$

30 and a power-law exponent of -0.64. In metamorphosed units, landslide D_{50} is also negatively correlated (with a larger scatter $R^2 = 0.5 - 0.55$) to landslide size metrics (area, width, volume, depth). However, we note that, for this dataset, these metrics are also strongly correlated with the drop height ($R^2 = 0.56 - 0.66$, Fig. S4). Therefore, these negative correlations between landslide size and GSD may not be causal, especially given that one may expect deeper landslides to mobilize fresher and coarser grains. We discuss in the next section a simple model for the landslide D_{50} combining a fragmentation scaling (Locat

Earth **Surface**
Dynamics
Discussions
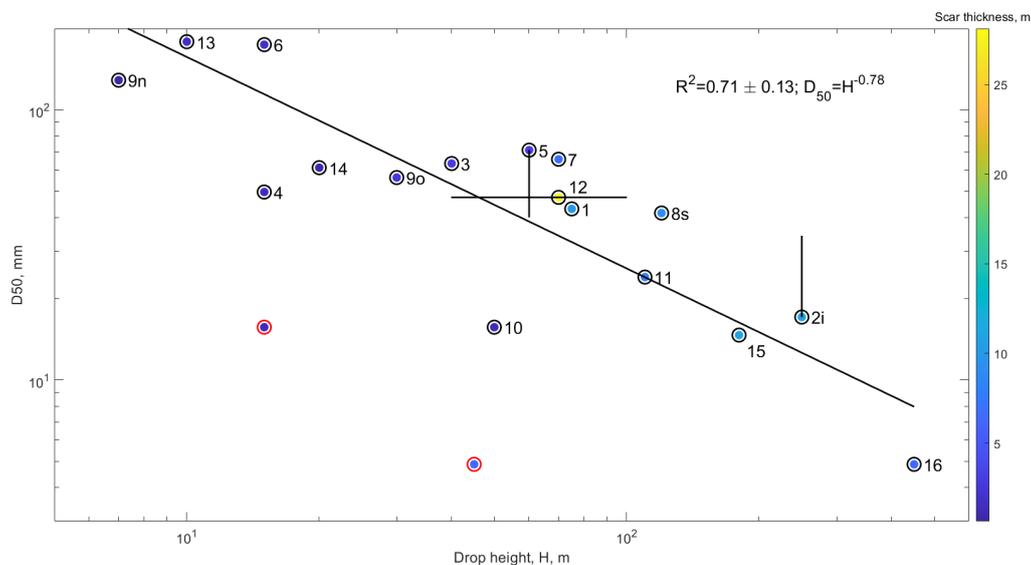
Figure 4. D_{50} for the 17 landslides (colorcoded by scar thickness) of this study against the drop height of their center of mass. Results are similar for maximal drop height. The best-fit (solid black line) and R^2 only consider the drop height rescaled by the landslide rock mass strength (black circles), about three and ten times weaker for LS-10 and LS-16 respectively (see methods). The red circles show the original drop height for these two landslides. Vertical bar show a factor of two uncertainty for LS-5 and LS-2i, for which there may be vertical segregation (see text).

et al., 2006) and a model for regolith coarsening with depth (Cohen et al., 2010).

For the spread of the distribution, characterized by the interquartile ratio, we did not find any substantial correlation with any of the landslide variable that we have constrained. Even the rock-type (or rock strength) does not seem to have an impact on the GSD spread, with several landslide in metasedimentary rocks with very large spreads (LS-3, LS-5, LS-1) and while the
5 two landslides in non-metamorphosed units are on both end of the spectrum. However, we note that, if the spread is almost uncorrelated to the D_{50} or D_{84}, it is substantially negatively correlated to the logarithm of D_{16} ($R^2 = 0.33 \pm 0.17$; $N = 17$) or in other words to the amount of fine grains (i.e., < 8 mm).

4 Discussion

A general limit of our study is that we rely on rough estimates of the landslide geometry (drop height, volume, depth, ...). Better
10 characterization in the field would have required more field work, and would have remained impossible for many landslides where the scar could not be accessed, or elaborate construction of DEM based on LIDAR or drone photogrammetry, difficult to perform and limited by the lack of accurate pre-failure DEMs. Thus for the sake of this first study we think that having a homogeneous, first-order estimates of these metrics is sufficient to test the dependence of the D_50 on landslide geometry. The

difficulty to access many scars, as well as the mixed origin (i.e., weathered regolith and bedrock) of several landslide sources also meant that in practice we could not measure the source materials median grain size, D_i. Nevertheless, we propose below that variability in D_i may be captured with existing weathering models.

4.1 The importance of fragmentation and source material initial grain size

5   Here we discuss the hypothesis that Eq (1) proposed and validated by Locat et al. (2006) for large rock avalanches can also be used for smaller, shallower landslides made of a mixture of regolith and bedrock. For the 17 Taiwanese landslide in our study we found that within a given lithology, drop height seems to be a first order control on the landslide deposit median grain size (Fig 4). We also found that by rescaling the drop height by their weaker rock strength, LS-10 an LS-16 were consistent with the trend defined by the stronger metamorphosed units. These observations qualitatively agree with Eq (1), but quantitatively,

10   the best fit between H and D_{50} was not linear, but a sub-linear power-law. Given that we observe that H and the landslide scar thickness, T, are correlated in our surveyed landslide (Fig S4) this discrepancy with Eq (1) could be resolved if D_i, which we could not measure, is increasing with T. Models describing the size of particles in a soil or regolith predict upwards fining of grains from the bedrock to the surface due to an increase in the degree of both physical and chemical weathering (Cohen et al., 2010; Anderson et al., 2013; Sklar et al., 2017). In bedrock, fracture density estimated from seismic wave refraction was also

15   found to decrease non-linearly from the surface to a depth of 5-10m (Clarke and Burbank, 2011). Given soils are often thin in Taiwan, and represented a small proportion of the mobilized material we consider physical weathering is likely dominant, and its intensity can be modelled with an exponential decay from the surface, with a characteristic length scale of $\lambda = 2\ m$, consistent with previous modeling works (Cohen et al., 2010; Anderson et al., 2013). Assuming the regolith grain size to be proportional to the integral of the weathering intensity, we modelled as $D_b(1 - exp(-z/\lambda))$ where z is the depth and D_b the

20   unweathered bedrock block size, producing a rapid variation near the surface consistent with published models for physical weathering (Cohen et al., 2010; Anderson et al., 2013). Imposing $D_b = 1900\ mm$, we obtained D_i for a given landslide by integrating this profile until, T, the mean scar thickness of the landslide (Fig 5a)

     The ratio of the modeled D_i and the measured D_{50} agree with Eq (1) ($R^2 = 0.9 \pm 0.05$), even though its coefficients (k_1 and k_2) were calibrated on rock avalanches with strength and median grain size order of magnitude larger than the ones from this

25   study (Table 1, Fig 2a, 5b). All of the surveyed landslides are within a factor of two from Eq (1), even LS-12 which likely had a different deformation style than the other landslides. Note that we chose $D_b = 1900\ mm$ to match the D_{50} measurements, which represent surface deposits. These may slightly over-estimate the representative grain size relative to the whole landslide deposit, because of kinetic sieving or fine removal by surface runoff (Fig 3C and discussion below). Based on LS-5 and 8, the inner D_{50} may be 2-3 times finer than their surface counterpart, and thus field measurement of regolith and bedrock GSD

30   may need to be compared to a model with $D_b \sim 600 - 1000\ mm$. We also note that LS-10 and 16 which occurred in weaker bedrock may be expected to have a finer D_b than the other slides. We are not able to constrain this but note that even with a D_b three times finer these two slides would be only a factor of 2 below the prediction (Fig 5).

We conclude this section by underlining that more measurements, especially of source rock block size and strength, are needed to fully demonstrate the applicability of the fragmentation theory presented by Locat et al. (2006). Still, we suggest that such
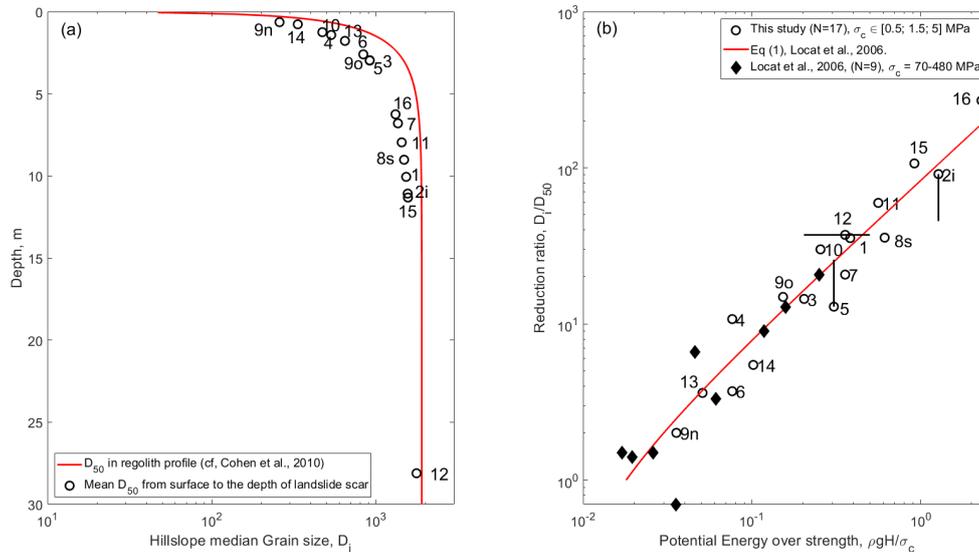
Figure 5. (a) Grain size as a function of depth in the regolith inspired by the weathering model by Cohen et al. (2010), used to estimate the original median grainsize, D_i mobilized by landslide with different thickness. (b) Reduction ratio (using the modeled D_i from (a)) against the potential energy normalized by point load strength for the 17 landslide deposits of this study.

fragmentation theory is applicable to understand and predict landslide GSD in a wide range of contexts, at least for rock, soil and mixed avalanches and generally disrupted slides, which are the most commonly triggered (Keefer, 1984). Further, our observations suggest that Eq 1 can be generalized to account for a exponential reduction of regolith grain size towards the surface (Cohen et al., 2010; Anderson et al., 2013), yielding:

$$D_{50} = \left(1 - \frac{\lambda}{T}(1 - e^{T/\lambda})\right) \frac{D_b}{k_1 \frac{\rho g H}{\sigma_c} - k_2} \qquad (2)$$

5   where D_i has been replaced by a term depending on the "fresh" bedrock median size, D_b, the length scale of weathering decay, and the landslide thickness. In a sense, Eq 2 supports previous qualitative statements on the importance of rock-type (Attal and Lavé, 2006; Roda-Boluda et al., 2018) which may physically relate to rock strength and regolith block size. Additionally, Eq 2 combines the concept of physical weathering, with the process of fragmentation, controlled by drop height, less often considered in the geomorphological community. More complex models of fragmentation have been used to predict landslide

10   GSD (De Blasio and Crosta, 2014; Ruiz-Carulla and Corominas, 2020), and may be better suited to model the full GSD, but Eq 2, provided it is further validated, opens various interesting perspectives. For example, it suggests that seismically triggered landslides, which occur more often near ridges than rainfall-triggered landslides (see Meunier et al., 2008; Rault et al., 2019), are more likely to deliver finer grains to the river systems, assuming they have a similar size and depth distributions. Eq 2 would also be well suited for landscape scale modeling of the input of various grain size into rivers (e.g., Benda and Dunne,

1997; Carretier et al., 2016; Neely and DiBiase, 2020), and thus, to better couple landslide and river dynamics in landscape evolution models (Campforts et al., 2020; Egholm et al., 2013).

4.2 Controls on the internal variability of the GSD and implications for future sampling

We found three sources of internal variability of landslide GSD, one associated with the lithology of the individual grains, as

5   reported for Himalayan landslides by Attal and Lavé (2006), and two related to the location of the grains on or in the deposit, as reported for various rock avalanches (Crosta et al., 2007; Ruiz-Carulla et al., 2015). We discuss these observations first in terms of implications for bias and sampling procedure, and second in terms of physical process causing them.

The lithological difference, is not likely to be a bias as long as the grains of different lithologies are randomly distributed in the deposit, their sampling frequency should represent their relative abundance in the deposit. Spatial segregation on the surface

10   of the deposit implies that to ensure a representative GSD, the sampling method should be performed ideally across most of the deposit, or at least over the different subunits of the deposit, before doing a weighted average with their relative area of contribution. Measurement based on a sieving at a single site or local grain counts along a line or over an area may misrepresent the GSD and should be avoided. For large deposit where access is difficult, the use of pictures from a drone may help to check for segregation and potentially allow to reproduce the grid-by-number counting method. However, this requires to scale each

15   drone picture, and thus to deploy reference objects across the deposit which is not always practical, not counting the fact that such sampling will be unable to resolve fine grains ($< 30 - 100\ mm$). In contrast, in the presence of a vertical segregation, where superficial and inner GSDs differ, it may be very difficult to estimate a GSD that is representative for the whole deposit. Some applications mainly require the subsurface GSD, for example modeling the weathering of freshly fragmented bedrock in the landslide deposit and how they can contribute to solute fluxes (Emberson et al., 2016a, b). In contrast, the surface grains

20   matter for sediment transport, and armoring may limit the mobilization of deeper finer grains. Additionally, in the case of a carapace, the question of how to combine the two end-member distribution would require an estimate of the relative thickness of the two end-member GSD, which may be challenging. In the case of a less extreme segregation, as observed for LS-8 and probably LS-5, the proportion of coarse grains ($> 200\ mm$) was similar on the surface and inside the deposit, and only the medium and especially fine grains were more abundant inside the deposit.

25

The process of kinetic sieving (Savage and Lun, 1988; Gray, 2018) is expected to cause vertical segregation (i.e., a coarser surface and finer subsurface) in granular flows, and a downslope segregation when shear is present, leading to boulder fronts as for LS-3. However, it should be noted that the segregation is favored by transport along moderate slope gradient and tends to disappear for very steep chutes (Vallance and Savage, 2000). Although our gradient estimates are very rough, the deposit with

30   segregation mostly occurred for landslides with large transport distance, estimated as $\sqrt{L^2 + H^2}$, and least steep slopes (Table 1, Fig. S5). This excludes LS-12 with likely a complex displacement, and LS-16 for which the weak and clay-rich lithology, prone to form agglomerate, may not have behaved like a typical granular material. Still, it seems hard to explain with kinetic sieving why LS-9n was so clearly segregated downslope, in spite of its very modest size and displacement. Instead, we could hypothesize that on some landslide deposit, episodic reactivation of the scar and channel chute may have sprayed the deposit

with finer debris, depositing preferentially near the apex of the deposit. Such mechanism might have happened on most of the landslide we have sampled (given their ages), but is hard to constrain its relevance without repeated monitoring of the deposits. Also, it depends heavily on the geometry, and is most likely for compact deposit below a steep, short chute, while on broad deposits below a moderately steep and long transport channel not much material is expected to reach the final deposit. Last,

5 for old deposit it is likely that fine materials could have been washed away by repeated storm events. This progressive washing of the fine grains would be consistent with the fact that the superficial deposits are very poor in fine materials, but have a proportion of coarse blocks fairly similar to the internal part of the deposit (for LS-5 and LS-8, Fig. 3). In these two cases, kinetic sieving may have been limited (although likely present in LS-8 to explain some downslope coarsening) and fines may have been preferentially washed out. On the deposit of LS-11 scraping the first layer of gravels in several locations we did find

10 finer materials, consistent with this hypothesis. If such a process is expected to happen on all landslides deposit, superficial measurement of very fresh landslide may already represent the bulk of the material (as perhaps LS-15 and LS-3, most recently failed and with high proportion of fine grains), and older deposit may require some correction as medium to fine grains may be underrepresented.

To conclude this discussion, it seems clear that several physical processes can complexify the landslide deposit GSD, and

15 that deconvolving them and applying a process-based correction to the GSD is not straightforward. More datasets are clearly needed to better understand these source of variability of the GSDs, for example with a more systematic sampling of very fresh landslides where fines should not have been washed out. Thus, we encourage such issue to be anticipated in future studies, and perform field work in a way allowing the spatial variability to be recorded. This would also enable future studies to include various landslide GSD based on different assumptions or corrections. In this sense, collecting more measurements of landslides

20 where both internal and superficial GSD can be measured seems essential, especially while trying to have very young landslides with similar characteristics (lithology, height drop).

4.3 Implications for sediment transport in Taiwan

The landslide GSD we report contain mainly gravel, but also a substantial fraction of boulders, which suggests that the transport and evacuation of the material will require large floods. To compare these GSDs to typical shear stresses occurring in Taiwanese

25 rivers, we use the shear stress map derived by Yanites et al. (2010b) from detailed measurement of the width, discharge and slope along the Peikang river. For a 10-year return flood with a discharge of $1000\ m^3.s^{-1}$, they found the shear stress ranged from $\tau \sim 60 - 400\ Pa$. To assess a threshold for bedload and suspended load transport, we computed for which grain size D the Shields number $\tau/(\rho/\rho_f - 1)gD$ was above a transport threshold of 0.045, and, for which D the shear velocity, estimated as $U_* = \sqrt{\tau/\rho_f}$, was larger than the settling velocity of the grain U_s as defined by Ferguson and Church (2004) (Fig. 2, 6).

30 Even for an above average 10-year return flood, less than 25% of most landslide deposits could be transported in suspension, except LS-10 and LS-16 with a suspended fraction of up to 50-70%. When accounting for bedload transport, the largest shear stress could not transport 5-25% of the deposits for about half of the landslides, especially LS-6, LS-9n and LS-13. However, considering smaller, but not uncommon, shear stresses (60-140 Pa) would result in an immobile fraction of 20 to 40% for most landslides, and up to 80% for the three coarsest deposits.

Before discussing the implications of this, we highlight three main limitations which should be addressed by future work aiming at constraining the export of landslides deposits. First, the shear stress could not be adjusted to the local channel conditions in which the landslide occurred. Second, armoring effects, in which a superficial layer of coarse grains inhibits the mobility of finer grains, were not considered. Armoring could be especially important when vertical or downslope segregation of grain

5   sizes is strong. Third, we did not consider debris-flows and hyper-concentrated flows, which are frequent in Taiwan (Dadson et al., 2005; Lin et al., 2005; Hsu et al., 2010), and which would enhance sediment transport given their higher fluid density. Despite these sources of uncertainty, our results suggest that in the relatively strong metasedimentary units, rapid evacuation of the sediment by suspension affects at most 30% of most of the deposits, and most of the transport occurs as bedload over a limited distance. Further, only the largest (10-year return or more) floods will transport substantial parts of the deposit, meaning

10   that large landslide events may load channels with a pulse of coarse sediments requiring several decades to be evacuated. This is much longer than the transient pulse of suspended sediment after the Chi-Chi earthquake, which affected river channels for less than 10 years (Hovius et al., 2011). This multi-decadal timescales for sediment export seems consistent with the very large alluviation of the Southern Taiwan river channel, that followed the Morakot intense flood and landsliding (Yanites et al., 2018), and which was still visible in 2015 (e.g., Taimali river), and at the time of writing in satellite imagery. Substantial aggradation,

15   suspected to be long-term, was also observed after the Chi-Chi earthquake (Yanites et al., 2010a; Chen, 2009). More detailed modeling of the evacuation of landslide sediment (e.g., Yanites et al., 2010a; Croissant et al., 2017) could be combined with scenarios based on the detailed GSD reported in this study to better quantify the dynamics and timescales of coarse sediment export after large landslides events.

5   Conclusions

20   We have presented grain-size distributions obtained from 17 landslide deposits in Taiwan. They have D_{50} and D_{84} consistent with previous literature, between 15-200 mm an 60-600 mm respectively. We found that many deposits had significant spatial segregation in the downslope directions, with the lowest part of the deposits having 2 to 10 times coarser GSDs than the upper part of the deposits. For the three landslides in which we could sample the inner part of deposits we also found GSDs 3 to 10 times finer than their surface counterparts. We did not find a single process which could explain the presence and intensity of

25   these segregation, though kinetic sieving and deposit reworking are likely candidates. Still, this internal variability is a strong caveat for very localized sampling (i.e., sieving from a single pit).

Investigating the controls on landslide GSD variability we observed a strong anticorrelations between the landslide drop height, width and inferred scar depths and the GSD percentiles for all the landslides. Finer GSDs in the two landslides in non-metamorphosed, young sedimentary rocks can be well explained by normalizing the drop height by the literature rock

30   strength. Further, modeling the source material median grain-size with an exponential fining towards the surface, consistent with physical weathering models, we found that the reduction ratio from source material to landslide deposits matches the scaling proposed by Locat et al. (2006) and calibrated for much larger and stronger rock avalanches than studied by us. Although future measurement on the source rock are needed for a complete demonstration, we suggests that simple geomorphic models

Earth **Surface**
Dynamics
Discussions
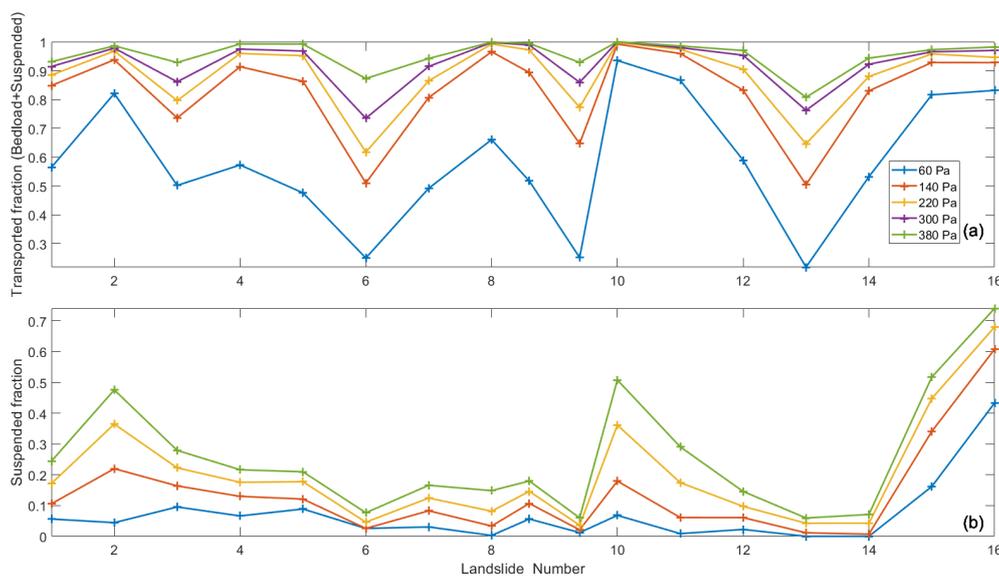
Figure 6. Fraction of the landslide GSD that could be transported as both bedload and suspended load (a) and only suspended load (b) as a function of river shear stress during a 10-year return flood. Note that in (b) suspended fraction at 300 and 380 MPa are identical.

coupling this fragmentation scaling with a model for regolith grainsize (see Eq 2) could be a physically-based 1st order model for the GSD input to rivers by landslides in active orogens. Such approach could have important implications for landscape evolution models and sediment transport. Indeed, from our deposits we also noted that even a 10-year flood may not be able to transport the coarsest fraction of many deposits, suggesting that floodplains will likely need several decades to recover after

5   large landslides event.

Data availability. The 28 GSD (for each landslide sub samples) are available in the Hydroshare open repository, together a shapefile with landslide locations and polygons derived from Google Earth. Marc, O., J. Turowski, P. Meunier (2021). Grain Size Distribution of 17 Taiwanese landslide deposits, HydroShare, http://www.hydroshare.org/resource/ade683be61e54fa5b60da97418a5f3df

Author contributions. OM designed the study and the field mission, performed all analyses and wrote the manuscript. JMT and PM provided
10   input for the field methodology, the result interpretations and edited the manuscript. All authors have been collecting the grain size data in the field.

Competing interests. The authors declare no competing interests

Acknowledgements. The grain counting during the 2015 field campaign could not have been possible without the additional participation of Antonius Golly, Arnaud Burtin, Anne Schöpa and Niels Hovius, and they are warmly thanked for this. We also thank Kristen Cook and Anne Schöpa for contributing pictures, and Sebastien Carretier for pointing us to the literature on physical weathering models.

References

Allen, P. A., Armitage, J. J., Whittaker, A. C., Michael, N. A., Roda-Boluda, D., and D'Arcy, M.: Fragmentation Model of the Grain Size Mix of Sediment Supplied to Basins, The Journal of Geology, 123, 405–427, https://doi.org/10.1086/683113, http://www.journals.uchicago.edu/doi/abs/10.1086/683113, 2015.

Anderson, R. S., Anderson, S. P., and Tucker, G. E.: Rock damage and regolith transport by frost: an example of climate modulation of the geomorphology of the critical zone, Earth Surface Processes and Landforms, 38, 299–316, https://doi.org/https://doi.org/10.1002/esp.3330, https://onlinelibrary.wiley.com/doi/abs/10.1002/esp.3330, _eprint: https://onlinelibrary.wiley.com/doi/pdf/10.1002/esp.3330, 2013.

Armitage, J. J., Duller, R. A., Whittaker, A. C., and Allen, P. A.: Transformation of tectonic and climatic signals from source to sedimentary archive, Nature Geoscience, 4, 231–235, https://doi.org/10.1038/ngeo1087, https://www.nature.com/articles/ngeo1087, number: 4 Publisher: Nature Publishing Group, 2011.

Attal, M. and Lavé, J.: Changes of bedload characteristics along the Marsyandi River (central Nepal): Implications for understanding hillslope sediment supply, sediment load evolution along fluvial networks, and denudation in active orogenic belts, Geological Society of America Special Papers, 398, 143–171, https://doi.org/10.1130/2006.2398(09), http://specialpapers.gsapubs.org/content/398/143, 2006.

Attal, M., Mudd, S. M., Hurst, M. D., Weinman, B., Yoo, K., and Naylor, M.: Impact of change in erosion rate and landscape steepness on hillslope and fluvial sediments grain size in the Feather River basin (Sierra Nevada, California), Earth Surface Dynamics, 3, 201–222, https://doi.org/https://doi.org/10.5194/esurf-3-201-2015, https://www.earth-surf-dynam.net/3/201/2015/, 2015.

Benda, L. and Dunne, T.: Stochastic forcing of sediment routing and storage in channel networks, Water Resources Research, 33, 2865–2880, https://doi.org/10.1029/97WR02387, http://onlinelibrary.wiley.com/doi/10.1029/97WR02387/abstract, 1997.

Campforts, B., Shobe, C. M., Steer, P., Vanmaercke, M., Lague, D., and Braun, J.: HyLands 1.0: a hybrid landscape evolution model to simulate the impact of landslides and landslide-derived sediment on landscape evolution, Geoscientific Model Development, 13, 3863–3886, https://doi.org/https://doi.org/10.5194/gmd-13-3863-2020, https://gmd.copernicus.org/articles/13/3863/2020/, publisher: Copernicus GmbH, 2020.

Carretier, S., Martinod, P., Reich, M., and Godderis, Y.: Modelling sediment clasts transport during landscape evolution, Earth Surface Dynamics, 4, 237–251, https://doi.org/10.5194/esurf-4-237-2016, http://www.earth-surf-dynam.net/4/237/2016/, 2016.

Casagli, N., Ermini, L., and Rosati, G.: Determining grain size distribution of the material composing landslide dams in the Northern Apennines: sampling and processing methods, Engineering Geology, 69, 83–97, https://doi.org/10.1016/S0013-7952(02)00249-1, http://www.sciencedirect.com/science/article/pii/S0013795202002491, 2003.

Chau, K. T. and Wong, R. H. C.: Uniaxial compressive strength and point load strength of rocks, International Journal of Rock Mechanics and Mining Sciences & Geomechanics Abstracts, 33, 183–188, https://doi.org/10.1016/0148-9062(95)00056-9, http://www.sciencedirect.com/science/article/pii/0148906295000569, 1996.

Chen, C.-Y.: Sedimentary impacts from landslides in the Tachia River Basin, Taiwan, Geomorphology, 105, 355–365, https://doi.org/10.1016/j.geomorph.2008.10.009, https://www.sciencedirect.com/science/article/pii/S0169555X08004637, 2009.

Chung, C.-H. and Chang, F.-J.: A refined automated grain sizing method for estimating river-bed grain size distribution of digital images, Journal of Hydrology, 486, 224–233, https://doi.org/10.1016/j.jhydrol.2013.01.026, http://www.sciencedirect.com/science/article/pii/S0022169413000723, 2013.

Clarke, B. A. and Burbank, D. W.: Quantifying bedrock-fracture patterns within the shallow subsurface: Implications for rock mass strength, bedrock landslides, and erodibility, Journal of Geophysical Research: Earth Surface, 116, F04 009, https://doi.org/10.1029/2011JF001987, http://onlinelibrary.wiley.com/doi/10.1029/2011JF001987/abstract, 2011.

Cohen, S., Willgoose, G., and Hancock, G.: The mARM3D spatially distributed soil evolution model: Three-dimensional model framework and analysis of hillslope and landform responses, Journal of Geophysical Research: Earth Surface, 115, https://doi.org/https://doi.org/10.1029/2009JF001536, https://agupubs.onlinelibrary.wiley.com/doi/abs/10.1029/2009JF001536, _eprint: https://agupubs.onlinelibrary.wiley.com/doi/pdf/10.1029/2009JF001536, 2010.

Cook, K. L., Turowski, J. M., and Hovius, N.: A demonstration of the importance of bedload transport for fluvial bedrock erosion and knickpoint propagation, Earth Surface Processes and Landforms, 38, 683–695, https://doi.org/10.1002/esp.3313, http://onlinelibrary.wiley.com/doi/10.1002/esp.3313/abstract, 2013.

Cook, K. L., Turowski, J. M., and Hovius, N.: River gorge eradication by downstream sweep erosion, Nature Geoscience, 7, 682–686, https://doi.org/10.1038/ngeo2224, https://www.nature.com/articles/ngeo2224, number: 9 Publisher: Nature Publishing Group, 2014.

Croissant, T., Lague, D., Steer, P., and Davy, P.: Rapid post-seismic landslide evacuation boosted by dynamic river width, Nature Geoscience, advance online publication, https://doi.org/10.1038/ngeo3005, https://www.nature.com/ngeo/journal/vaop/ncurrent/full/ngeo3005.html, 2017.

Crosta, G. B., Frattini, P., and Fusi, N.: Fragmentation in the Val Pola rock avalanche, Italian Alps, Journal of Geophysical Research: Earth Surface, 112, F01 006, https://doi.org/10.1029/2005JF000455, http://onlinelibrary.wiley.com/doi/10.1029/2005JF000455/abstract, 2007.

Dadson, S., Hovius, N., Pegg, S., Dade, W. B., Horng, M. J., and Chen, H.: Hyperpycnal river flows from an active mountain belt, Journal of Geophysical Research: Earth Surface, 110, https://doi.org/https://doi.org/10.1029/2004JF000244, https://agupubs.onlinelibrary.wiley.com/doi/abs/10.1029/2004JF000244, _eprint: https://agupubs.onlinelibrary.wiley.com/doi/pdf/10.1029/2004JF000244, 2005.

De Blasio, F. V. and Crosta, G. B.: Simple physical model for the fragmentation of rock avalanches, Acta Mechanica, 225, 243–252, https://doi.org/10.1007/s00707-013-0942-y, http://link.springer.com/article/10.1007/s00707-013-0942-y, 2014.

Domej, G., Bourdeau, C., and Lenti, L.: Mean Landslide Geometries Inferred from a Global Database of Earthquake- and Non-Earthquake-Triggered Landslides, Italian Journal of Engineering Geology and Environment, pp. 87–107, https://doi.org/10.4408/IJEGE.2017-02.O-05, http://www.ijege.uniroma1.it/rivista/ijege-17/ijege-17-volume-02/mean-landslide-geometries-inferred-from-a-global-database-of-earthquake-and-non-earthquake-triggered-landslides/ijege-17_02-domej-et-alii.pdf, 2017.

Egholm, D. L., Knudsen, M. F., and Sandiford, M.: Lifespan of mountain ranges scaled by feedbacks between landsliding and erosion by rivers, Nature, 498, 475–478, https://doi.org/10.1038/nature12218, https://www.nature.com/nature/journal/v498/n7455/full/nature12218.html, 2013.

Emberson, R., Hovius, N., Galy, A., and Marc, O.: Chemical weathering in active mountain belts controlled by stochastic bedrock landsliding, Nature Geoscience, 9, 42–45, https://doi.org/10.1038/ngeo2600, http://www.nature.com/ngeo/journal/vaop/ncurrent/full/ngeo2600.html#contrib-auth, 2016a.

Emberson, R., Hovius, N., Galy, A., and Marc, O.: Oxidation of sulfides and rapid weathering in recent landslides, Earth Surface Dynamics, 4, 727–742, https://doi.org/https://doi.org/10.5194/esurf-4-727-2016, https://www.earth-surf-dynam.net/4/727/2016/, 2016b.

Ferguson, R. I. and Church, M.: A Simple Universal Equation for Grain Settling Velocity, Journal of Sedimentary Research, 74, 933–937, https://doi.org/10.1306/051204740933, http://jsedres.geoscienceworld.org/content/74/6/933, 2004.

Gray, J. M. N. T.: Particle Segregation in Dense Granular Flows, Annual Review of Fluid Mechanics, 50, 407–433, https://doi.org/10.1146/annurev-fluid-122316-045201, https://doi.org/10.1146/annurev-fluid-122316-045201, _eprint: https://doi.org/10.1146/annurev-fluid-122316-045201, 2018.

Guerit, L., Barrier, L., Narteau, C., Métivier, F., Liu, Y., Lajeunesse, E., Gayer, E., Meunier, P., Malverti, L., and Ye, B.: The Grain-size Patchiness of Braided Gravel-Bed Streams – example of the Urumqi River (northeast Tian Shan, China), in: Advances in Geosciences, vol. 37, pp. 27–39, Copernicus GmbH, https://doi.org/https://doi.org/10.5194/adgeo-37-27-2014, https://adgeo.copernicus.org/articles/37/27/2014/, iSSN: 1680-7340, 2014.

Guerit, L., Barrier, L., Liu, Y., Narteau, C., Lajeunesse, E., Gayer, E., and Métivier, F.: Uniform grain-size distribution in the active layer of a shallow, gravel-bedded, braided river (the Urumqi River, China) and implications for paleo-hydrology, Earth Surface Dynamics, 6, 1011–1021, https://doi.org/https://doi.org/10.5194/esurf-6-1011-2018, https://esurf.copernicus.org/articles/6/1011/2018/, publisher: Copernicus GmbH, 2018.

Hovius, N., Stark, C. P., and Allen, P. A.: Sediment flux from a mountain belt derived by landslide mapping, Geology, 25, 231–234, https://doi.org/10.1130/0091-7613(1997)025<0231:SFFAMB>2.3.CO;2, http://geology.geoscienceworld.org/content/25/3/231, 1997.

Hovius, N., Stark, C. P., Chu, H., and Lin, J.: Supply and Removal of Sediment in a Landslide Dominated Mountain Belt: Central Range, Taiwan, The Journal of Geology, 108, 73–89, https://doi.org/10.1086/jg.2000.108.issue-1, http://www.jstor.org/stable/10.1086/314387, 2000.

Hovius, N., Meunier, P., Lin, C., Chen, H., Chen, Y., Dadson, S., Horng, M., and Lines, M.: Prolonged seismically induced erosion and the mass balance of a large earthquake, Earth and Planetary Science Letters, 304, 347–355, https://doi.org/10.1016/j.epsl.2011.02.005, 2011.

Hsu, S. M., Chiou, L. B., Lin, G. F., Chao, C. H., Wen, H. Y., and Ku, C. Y.: Applications of simulation technique on debris-flow hazard zone delineation: a case study in Hualien County, Taiwan, Natural Hazards and Earth System Sciences, 10, 535–545, https://doi.org/https://doi.org/10.5194/nhess-10-535-2010, https://nhess.copernicus.org/articles/10/535/2010/nhess-10-535-2010.html, publisher: Copernicus GmbH, 2010.

Ibbeken, H.: Jointed source rock and fluvial gravels controlled by Rosin's law; a grain-size study in Calabria, South Italy, Journal of Sedimentary Research, 53, 1213–1231, https://doi.org/10.1306/212F834B-2B24-11D7-8648000102C1865D, https://pubs.geoscienceworld.org/sepm/jsedres/article-abstract/53/4/1213/97681/Jointed-source-rock-and-fluvial-gravels-controlled, publisher: GeoScienceWorld, 1983.

Keefer, D. K.: Landslides caused by earthquakes, Geological Society of America Bulletin, 95, 406–421, https://doi.org/10.1130/0016-7606(1984)95<406:LCBE>2.0.CO;2, http://gsabulletin.gsapubs.org/content/95/4/406, 1984.

Kellerhals, R. and Bray, D. I.: Sampling Procedures for Coarse Fluvial Sediments, Journal of the Hydraulics Division, 97, 1165–1180, http://cedb.asce.org/cgi/WWWdisplay.cgi?18017, 1971.

Larsen, I., Montgomery, D., and Korup, O.: Landslide erosion controlled by hillslope material, Nature Geoscience, 3, 247–251, 2010.

Lin, C.-P., Wang, Y.-M., Tfwala, S. S., and Chen, C.-N.: The Variation of Riverbed Material due to Tropical Storms in Shi-Wen River, Taiwan, The Scientific World Journal, https://doi.org/https://doi.org/10.1155/2014/580936, https://www.hindawi.com/journals/tswj/2014/580936/, iSSN: 2356-6140 Pages: e580936 Publisher: Hindawi Volume: 2014, 2014.

Lin, G.-W., Chen, H., Hovius, N., Horng, M.-J., Dadson, S., Meunier, P., and Lines, M.: Effects of earthquake and cyclone sequencing on landsliding and fluvial sediment transfer in a mountain catchment, Earth Surface Processes and Landforms, 33, 1354–1373, https://doi.org/10.1002/esp.1716, http://onlinelibrary.wiley.com/doi/10.1002/esp.1716/abstract, 2008.

Lin, M.-L., Wang, K.-L., and Huang, J.-J.: Debris flow run off simulation and verification - case study of Chen-You-Lan Watershed, Tai-wan, Natural Hazards and Earth System Sciences, 5, 439–445, https://doi.org/https://doi.org/10.5194/nhess-5-439-2005, https://nhess.copernicus.org/articles/5/439/2005/, publisher: Copernicus GmbH, 2005.

Locat, P., Couture, R., Leroueil, S., Locat, J., and Jaboyedoff, M.: Fragmentation energy in rock avalanches, Canadian Geotechnical Journal, 43, 830–851, https://doi.org/10.1139/t06-045, http://www.nrcresearchpress.com/doi/abs/10.1139/t06-045, 2006.

Marc, O., Stumpf, A., Malet, J.-P., Gosset, M., Uchida, T., and Chiang, S.-H.: Initial insights from a global database of rainfall-induced landslide inventories: the weak influence of slope and strong influence of total storm rainfall, Earth Surface Dynamics, 6, 903–922, https://doi.org/https://doi.org/10.5194/esurf-6-903-2018, https://www.earth-surf-dynam.net/6/903/2018/, 2018.

Marc, O., Behling, R., Andermann, C., Turowski, J. M., Illien, L., Roessner, S., and Hovius, N.: Long-term erosion of the Nepal Himalayas by bedrock landsliding: the role of monsoons, earthquakes and giant landslides, Earth Surface Dynamics, 7, 107–128, https://doi.org/https://doi.org/10.5194/esurf-7-107-2019, https://www.earth-surf-dynam.net/7/107/2019/#&gid=1&pid=1, 2019.

Marshall, J. A. and Sklar, L. S.: Mining soil databases for landscape-scale patterns in the abundance and size distribution of hillslope rock fragments, Earth Surface Processes and Landforms, 37, 287–300, https://doi.org/10.1002/esp.2241, http://onlinelibrary.wiley.com/doi/10.1002/esp.2241/abstract, 2012.

Meunier, P., Hovius, N., and Haines, J. A.: Topographic site effects and the location of earthquake induced landslides, Earth and Planetary Science Letters, 275, 221–232, https://doi.org/10.1016/j.epsl.2008.07.020, http://www.sciencedirect.com/science/article/pii/S0012821X08004536, 2008.

Neely, A. B. and DiBiase, R. A.: Drainage Area, Bedrock Fracture Spacing, and Weathering Controls on Landscape-Scale Patterns in Surface Sediment Grain Size, Journal of Geophysical Research: Earth Surface, 125, e2020JF005560, https://doi.org/https://doi.org/10.1029/2020JF005560, https://agupubs.onlinelibrary.wiley.com/doi/abs/10.1029/2020JF005560, _eprint: https://agupubs.onlinelibrary.wiley.com/doi/pdf/10.1029/2020JF005560, 2020.

Nishiguchi, Y., Uchida, T., Takezawa, N., Ishizuka, T., and Mizuyama, T.: Runout Characteristics and Grain Size Distribution of Large-scale Debris Flows Triggered by Deep Catastrophic Landslides, International Journal of Erosion Control Engineering, 5, 16–26, https://doi.org/10.13101/ijece.5.16, 2012.

Rault, C., Robert, A., Marc, O., Hovius, N., and Meunier, P.: Seismic and geologic controls on spatial clustering of landslides in three large earthquakes, Earth Surface Dynamics, 7, 829–839, https://doi.org/https://doi.org/10.5194/esurf-7-829-2019, https://www.earth-surf-dynam.net/7/829/2019/, 2019.

Riebe, C. S., Sklar, L. S., Lukens, C. E., and Shuster, D. L.: Climate and topography control the size and flux of sediment produced on steep mountain slopes, Proceedings of the National Academy of Sciences, 112, 15 574–15 579, https://doi.org/10.1073/pnas.1503567112, https://www.pnas.org/content/112/51/15574, publisher: National Academy of Sciences Section: Physical Sciences, 2015.

Roda-Boluda, D. C., D'Arcy, M., McDonald, J., and Whittaker, A. C.: Lithological controls on hillslope sediment supply: insights from landslide activity and grain size distributions, Earth Surface Processes and Landforms, 43, 956–977, https://doi.org/10.1002/esp.4281, https://onlinelibrary.wiley.com/doi/abs/10.1002/esp.4281, _eprint: https://onlinelibrary.wiley.com/doi/pdf/10.1002/esp.4281, 2018.

Ruiz-Carulla, R. and Corominas, J.: Analysis of Rockfalls by Means of a Fractal Fragmentation Model, Rock Mechanics and Rock Engineering, 53, 1433–1455, https://doi.org/10.1007/s00603-019-01987-2, https://doi.org/10.1007/s00603-019-01987-2, 2020.

Ruiz-Carulla, R., Corominas, J., and Mavrouli, O.: A methodology to obtain the block size distribution of fragmental rockfall deposits, Landslides, 12, 815–825, https://doi.org/10.1007/s10346-015-0600-7, https://doi.org/10.1007/s10346-015-0600-7, 2015.

Savage, S. B. and Lun, C. K. K.: Particle size segregation in inclined chute flow of dry cohesionless granular solids, Journal of Fluid Mechanics, 189, 311–335, https://doi.org/10.1017/S002211208800103X, https://www.cambridge.org/core/journals/journal-of-fluid-mechanics/article/particle-size-segregation-in-inclined-chute-flow-of-dry-cohesionless-granular-solids/BD675CAD1F018B90E62A99E070296D68, publisher: Cambridge University Press, 1988.

5   Sklar, L. S. and Dietrich, W. E.: Sediment and rock strength controls on river incision into bedrock, Geology, 29, 1087–1090, https://doi.org/10.1130/0091-7613(2001)029<1087:SARSCO>2.0.CO;2, https://doi.org/10.1130/0091-7613(2001)029<1087:SARSCO>2.0.CO;2, 2001.

Sklar, L. S., Riebe, C. S., Marshall, J. A., Genetti, J., Leclere, S., Lukens, C. L., and Merces, V.: The problem of predicting the size distribution of sediment supplied by hillslopes to rivers, Geomorphology, 277, 31–49, https://doi.org/10.1016/j.geomorph.2016.05.005,
10   http://www.sciencedirect.com/science/article/pii/S0169555X16302690, 2017.

Stephens, M. A.: EDF Statistics for Goodness of Fit and Some Comparisons, Journal of the American Statistical Association, 69, 730–737, https://doi.org/10.2307/2286009, https://www.jstor.org/stable/2286009, publisher: [American Statistical Association, Taylor & Francis, Ltd.], 1974.

Struck, M., Andermann, C., Hovius, N., Korup, O., Turowski, J. M., Bista, R., Pandit, H. P., and Dahal, R. K.: Monsoonal hillslope processes
15   determine grain size-specific suspended sediment fluxes in a trans-Himalayan river: Mass wasting determines sediment caliber, Geophysical Research Letters, 42, 2302–2308, https://doi.org/10.1002/2015GL063360, http://doi.wiley.com/10.1002/2015GL063360, 2015.

Turowski, J. M.: Alluvial cover controlling the width, slope and sinuosity of bedrock channels, Earth Surface Dynamics, 6, 29–48, https://doi.org/https://doi.org/10.5194/esurf-6-29-2018, https://esurf.copernicus.org/articles/6/29/2018/, publisher: Copernicus GmbH, 2018.

20   Vallance, J. W. and Savage, S. B.: Particle Segregation in Granular Flows Down Chutes, in: IUTAM Symposium on Segregation in Granular Flows, edited by Rosato, A. D. and Blackmore, D. L., pp. 31–51, Springer Netherlands, Dordrecht, 2000.

Whittaker, A. C., Duller, R. A., Springett, J., Smithells, R. A., Whitchurch, A. L., and Allen, P. A.: Decoding downstream trends in stratigraphic grain size as a function of tectonic subsidence and sediment supply, GSA Bulletin, 123, 1363–1382, https://doi.org/10.1130/B30351.1, https://pubs.geoscienceworld.org/gsa/gsabulletin/article/123/7-8/1363/125680/
25   Decoding-downstream-trends-in-stratigraphic-grain, publisher: GeoScienceWorld, 2011.

Yanites, B., Tucker, G., Mueller, K., and Chen, Y.: How rivers react to large earthquakes: Evidence from central Taiwan, Geology, 38, 639–642, 2010a.

Yanites, B. J., Tucker, G. E., Mueller, K. J., Chen, Y.-G., Wilcox, T., Huang, S.-Y., and Shi, K.-W.: Incision and channel morphology across active structures along the Peikang River, central Taiwan: Implications for the importance of channel width, GSA Bul-
30   letin, 122, 1192–1208, https://doi.org/10.1130/B30035.1, https://pubs.geoscienceworld.org/gsa/gsabulletin/article-abstract/122/7-8/1192/125575/Incision-and-channel-morphology-across-active, publisher: GeoScienceWorld, 2010b.

Yanites, B. J., Mitchell, N. A., Bregy, J. C., Carlson, G. A., Cataldo, K., Holahan, M., Johnston, G. H., Nelson, A., Valenza, J., and Wanker, M.: Landslides control the spatial and temporal variation of channel width in southern Taiwan: Implications for landscape evolution and cascading hazards in steep, tectonically active landscapes, Earth Surface Processes and
35   Landforms, 43, 1782–1797, https://doi.org/https://doi.org/10.1002/esp.4353, https://onlinelibrary.wiley.com/doi/abs/10.1002/esp.4353, _eprint: https://onlinelibrary.wiley.com/doi/pdf/10.1002/esp.4353, 2018.